Visible Infrared Imaging Radiometer Suite (VIIRS) 750 m Active Fire Detection and Characterization Algorithm Theoretical Basis Document 1.0

September 2017

Table of Contents

Written by:

Wilfrid Schroeder & Louis Giglio
Department of Geographical Sciences
University of Maryland
Email: wschroed@umd.edu

1. SCIENCE RATIONALE FOR THE PRODUCT

This document describes the baseline Visible Infrared Imaging Radiometer Suite (VIIRS) 750 m active fire detection product. The VIIRS instrument was first launched on 28 October 2011 onboard the Suomi National Polar-orbiting Partnership (S-NPP), which was placed in a sun synchronous orbit at an altitude of 829 km and with 1:30pm/1:30am equatorial crossing times. That instrument will be followed by other similar sensors onboard the Joint Polar Satellite System (JPSS) series of satellites operated jointly by NASA and NOAA. VIIRS is a whiskbroom scanning radiometer with a swath width of 3060 km, providing global wall-to-wall coverage every 12 h or less depending on the latitude. It consists of a multispectral instrument including five spectral channels (0.6 <> 12.4 μm) at 375 m (I-bands) and 16 spectral channels (0.4 <> 12.5 μm) at 750 m (M-bands), in addition to a light-sensitive (0.5 <> 0.9 μm) day-and-night band at 750 m (DNB).

The VIIRS 750 m active fire algorithm is an adaptation of the MODIS Collection 6 *Fire and Thermal Anomalies* product (MOD14/MYD14) [Giglio *et al.*, 2016]. The same algorithm formulation was implemented for VIIRS, with relatively small/straightforward changes made to the input/output routines in order to accommodate the particular NetCDF4.2/HDF5 data format. The VIIRS 750 m active fire detection and characterization data was originally conceived as part of VIIRS land product suite; it provides continuity to the 1 km Earth Observing System Moderate Resolution Imaging Spectroradiometer (EOS/MODIS) active fire data record.

2. THE ALGORITHM

2.1. TECHNICAL BACKGROUND AND HERITAGE

Actively burning fires often show a wide range of temperatures spanning several hundred Kelvin in association with flaming and smoldering phases of combustion. Typically, cooler smoldering fires show temperatures between 450 and 850 K, whereas higher temperatures ranging from 800 K to upwards of 1200 K prevail during the more intense flaming phase [Lobert and Warnatz, 1993]. Fuel type and moisture, and ambient conditions (air temperature, wind, and relative humidity) are key factors regulating biomass combustion. When moderate spatial resolution sensors are considered, mid-infrared (4 μm) spectral channels are the most responsive to actively burning fires capturing most of the radiometric signal from smoldering and flaming phases of combustion during both day and nighttime parts of the orbit. The peak in emitted fire radiant energy on channel M13 makes that channel responsive to small sub-pixel fires occurring over a cool (≤ 300 K) background. Consequently, intense active fires (>1000 K) occupying fractional pixel areas as small as 10^{-4} may be detected. In addition to facilitating the detection of sub-pixel active fires, the rate of radiative energy released by fires observed in the 4 μm region is found to be directly related to the biomass consumed per unit time [Kaufman *et al.*, 1998; Wooster *et al.*, 2003].

The baseline VIIRS 750 m active fire detection product was originally designed mirroring the MODIS Collection 4 *Fire and Thermal Anomalies* algorithm (MOD14/MYD14), although lacking key output science data layers such as the 2D fire mask and FRP retrievals [Csiszar *et al.*, 2014; Giglio *et al.*, 2003]. That algorithm was later replaced with the MODIS Collection 6 algorithm equivalent including all output science data layers [Giglio *et al.*, 2016]. That product is available through various VIIRS data outlets providing direct readout (NASA's International Polar Orbiter Processing Package [IPOPP]), near real-time (NOAA's S-NPP Data Exploitation [NDE]), and science data access (NASA's Land Science Investigator-led Processing System [Land SIPS]). An alternative VIIRS active fire product was since developed using the complementary 375 m channels [Schroeder *et al.*, 2014]. Given the higher spatial resolution of that product, improved fire detection performance is normally observed compared to the 750 m fire product version. Users are encouraged to consult the documentation describing the two products when choosing the most appropriate data set for their particular applications. The VIIRS 750 m fire product generation and availability will continue until further notice.

2.2. ALGORITHM INPUT

The VIIRS 750 m fire product uses input data from six 750 m channels, in addition to their corresponding quality flags (QF1) and geolocation data (Table 1).

Table 1: List of VIIRS channels used as input to the 750 m active fire detection algorithm. The corresponding VIIRS Level 1B data quality flags, terrain-corrected geolocation and quarterly land-water mask data complement the list of input files used.

VIIRS Channels	Heritage MODIS Channels	Primary Use
M5 (0.662 – 0.682 μm)	**1** (0.620 – 0.670 μm)	Cloud masking, Sun glint and false alarm rejection
M7 (0.846 – 0.885 μm)	**2** (0.841 – 0.876 μm)	Cloud masking, Sun glint and false alarm rejection
M11 (2.225 – 2.275 μm)	**7** (2.105 – 2.155 μm)	Sun glint and false alarm rejection
M13 (3.973 – 4.128 μm)	**21/22** (3.929 – 3.989 μm)	Fire detection and characterization
M15 (10.263 – 11.263 μm)	**31** (10.780 – 11.280 μm)	Fire detection, cloud masking, false alarm rejection
M16 (11.538 – 12.488 μm)	**32** (11.770 – 12.270 μm)	Cloud masking

The 750 m data describe the nominal resolution after native pixels are spatially aggregated (Figure 1). The aggregation scheme changes across three distinct image regions. In the first region (nadir to 31.59^o scan angle), three native pixels are aggregated in the along scan (cross-track) direction to form one data sample in the Level 1 image. In the second region (31.59^o to 44.68^o scan angle), two native pixels are aggregated to form one data sample. Finally in the third and last region (44.68^o to 56.06^o - edge of swath) one native pixel will result in one data sample. Single gain channels M11, M15 and M16 are aggregated onboard the

spacecraft before the data are transmitted to the ground stations. The dual-gain channels M5, M7 and M13 channel data undergo a similar aggregation scheme although the data reduction is performed after the ground stations receive the native resolution data from the satellite. The VIIRS 750 m fire algorithm uses aggregated data from all input channels.
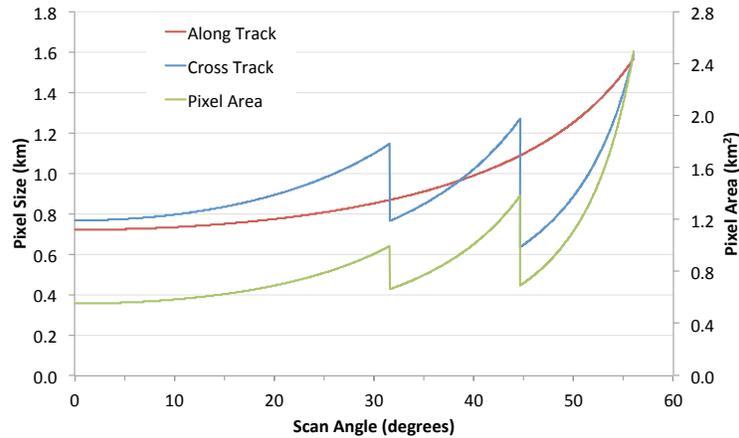

Figure 1: Spatial resolution of VIIRS radiometer data (M bands) as a function of scan angle. The three distinct regions describe data aggregation zones extending from nadir to the edge of the swath.

The dual-gain M13 channel is the primary input data to the fire detection and characterization routines. Compared to MODIS low and high gain channels 21 and 22, VIIRS M13 channel uses dynamically-assigned low/high gain settings depending the pixel radiance level. The saturation temperature on VIIRS M13 channel is approximately 659 K (compared to 500 K on MODIS channel 21); pixel saturation is extremely rare and normally limited to very large and intense wildfires. Saturation is accompanied by corresponding quality flags indicating full or partial saturation depending on the data aggregation scenario.

Currently, processing of the fire algorithm is limited to the Level 2 (swath) product output, which has similar data structure and format to MODIS Level 2 (MOD14/MYD14) fire product. It includes a two-dimensional fire mask and quality assurance science data sets, plus sparse arrays describing individual fire pixel information (e.g., FRP) and additional granule attributes. Supplementary Level 3 (tiled) and 4 (Climate Modeling Grid) product outputs may be added in the future.

2.3. ALGORITHM DESCRIPTION

The VIIRS 750 m fire algorithm uses a combination of fixed and contextual tests to detect active fires and other thermal anomalies in both daytime and nighttime (solar zenith angle ≥ 85º) parts of the orbit. The current implementation is essentially identical to the MODIS Collection 6 *Fire and Thermal Anomalies* (MOD14/MYD14) product. Users are referred to Giglio *et al*. [2016] for a detailed description of the active fire detection tests and sub-pixel fire characterization procedures involved.

4

That publication is downloadable free of charge through the link:
http://dx.doi.org/10.1016/j.rse.2016.02.054

3. PRODUCT DESCRIPTION

The VIIRS land product suite is composed of Level 2 (swath projection), Level 3 (tiled, with some multi-temporal data), and Level 4 (gridded data meeting climate modeling community requirements) data sets. Currently, the 750 m active fire data set is restricted to Level 2 processing carrying similar characteristics as the input L1B data ingested by the algorithm. The data are stored in swath projection with individual granules comprising an orbit segment of approximately 6 min. VIIRS Level 3 & 4 fire data products should become available in the near future.

3.1. LEVEL 2 ACTIVE FIRE DATA

3.1.1. FILE FORMAT

VIIRS active fire data are output in NetCDF4.2 file format. Level 2 files also share several of the L1B global attributes (including nomenclature); files can be manipulated using standard NetCDF-enabled software. Filename convention is as follows:

VNP14.AYYYYDDD.HHMM.VVV.yyyydddhhmmss.nc
Where:
VNP14 = VIIRS 750 m active fire product identifier
YYYY = year of data acquisition
DDD = Julian day of data acquisition
HHMM = hour and minute of data acquisition
yyyydddhhmmss = data processing time (year, Julian day, hour, minute, second)

3.1.2. DATA CONTENT

The VIIRS active fire algorithm output contains 29 primary science data sets, in addition to the algorithm's quality flag (see Section 3.2). The individual science data sets (SDSs) are named as follows:

'*fire mask*'   = image classification array (2D)
'*FP_line*'   = granule line of fire pixel
'*FP_sample*'   = granule sample of fire pixel
'*FP_latitude*'   = latitude of fire pixel (degrees)
'*FP_longitude*'= longitude of fire pixel (degrees)
'*FP_R7*'   = channel M7 reflectance of fire pixel
'*FP_T13*'   = channel M13 brightness temperature of fire pixel (kelvin)
'*FP_T15*'   = channel M15 brightness temperature of fire pixel (kelvin)
'*FP_MeanT13*' = channel M13 mean background brightness temperature (kelvin)
'*FP_MeanT15*' = channel M15 mean background brightness temperature (kelvin)

'*FP_MeanDT*' = mean background M13-M15 brightness temperature difference (kelvin)

'*FP_MAD_T13*' = background channel M13 brightness temperature mean absolute deviation (kelvin)

'*FP_MAD_T15*' = background channel M15 brightness temperature mean absolute deviation (kelvin)

'*FP_MAD_DT*' = background M13-M15 brightness temperature difference mean absolute deviation (kelvin)

'*FP_power*' = fire radiative power (MW)

'*FP_AdjCloud*' = number of adjacent cloud pixels

'*FP_AdjWater*' = number of adjacent water pixels

'*FP_WinSize*' = number of adjacent water pixels

'*FP_NumValid*' = number of valid background pixels

'*FP_confidence*' = detection confidence (7=low, 8=nominal, 9=high)

'*FP_land*' = land pixel flag

'*FP_MeanR7*' = background channel M7 reflectance

'*FP_MAD_R7*' = background channel M7 reflectance mean absolute deviation

'*FP_ViewZenAng*' = view zenith angle of fire pixel (degrees)

'*FP_SolZenAng*' = solar zenith angle of fire pixel (degrees)

'*FP_RelAzAng*' = relative azimuth angle of fire pixel (degrees)

'*FP_CMG_row*' = climate modeling grid row (used for CMG product generation)

'*FP_CMG_rol*' = climate modeling grid column (used for CMG product generation)

'*FP_CMG_day*' = day flag (used for CMG product generation)

'*FP_CMG_night*' = night flag (used for CMG product generation)

The '*fire mask*' SDS consists of an 8-bit integer two-dimensional array with the same number of elements as the input L1B data array (Figure 2). Fire masks generated from the standard 6-minute files have 3,200 samples (constant) and 202 <> 203 scans totaling 3,232 <> 3,248 rows (variable number of scans per granule is designed to accommodate ≈6 minute data segments). Distinct pixel classes are used for land, water, cloud and fire pixels, plus additional classes indicating non-processed pixels and pixels with undefined classification ('*unclassified*') (Table 2). The latter describes those cases when background statistics cannot be retrieved preventing proper pixel classification. Fire pixel confidence classes ('*low*', '*nominal*' and '*high*') are representative of the observation conditions associated with each detection. The additional data sets output by the algorithm consist of individual sparse arrays containing image line, column, longitude, latitude, FRP, detection confidence, among other parameters for all fire pixels detected.
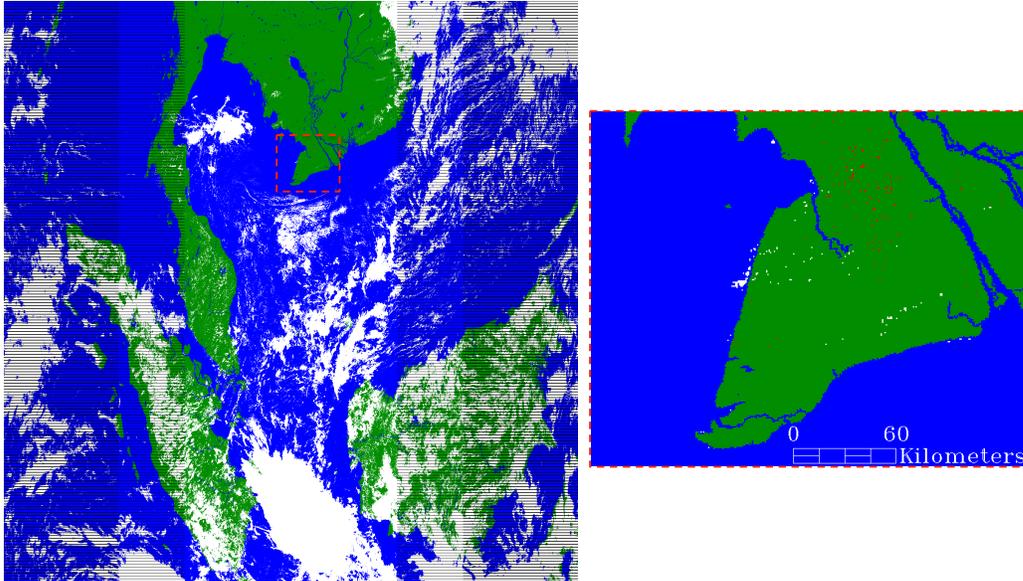
Figure 2: S-NPP/VIIRS 750 m active fire detection classification product (mask) derived for a 6-min granule acquired on 01 March 2016 at 0618 UTC over parts of Southeast Asia. Right panel shows magnified subset containing land (green), water (blue), clouds (white) and fire (red) pixels.

Table 2: VIIRS 750 m '*fire mask*' data set classes.

Pixel Class	Definition
0	Not processed
1	*Bowtie* deletion
2	(not being used)
3	Water
4	Clouds
5	Land
6	Unclassified
7	Low confidence fire pixel
8	Nominal confidence fire pixel
9	High confidence fire pixel

3.2. QA/METADATA

A two-dimensional array complements the fire mask output providing quality assurance (QA) information for every pixel processed. The QA data are stored in 32-bit unsigned integer format populated with several fields that together can be used to reconstruct some of the key observation conditions pertinent to each pixel analyzed.

Table 3: VIIRS 750 m fire detection '*algorithm QA*' data set bits and definition.

Bit	Description
0-1	land/water state (00 = water, 01 = coast, 10 = land, 11 = unused)
2	EDR ground trim zone (0= false, 1 = true)
3	atmospheric correction performed (0 = no, 1 = yes)
4	day/night algorithm (0 = night, 1 = day)
5	potential fire pixel (0 = false, 1 = true)
6	spare (set to 0)

7-10	background window size parameter
11-16	individual detection test flags (0 = fail, 1 = pass)
17-19	spare (set to 0)
20	adjacent cloud pixel (0 = no, 1 = yes)
21	adjacent water pixel (0 = no, 1 = yes)
22-23	Sun glint level (0-3)
24-28	individual rejection test flags (0 = false, 1 = true)
29-31	spare (set to 0)

4. PRODUCT ASSESSMENT

4.1. THEORETICAL FIRE DETECTION CURVES

A theoretical fire detection envelope was calculated by simulating fire activity in a boreal ecosystem using the methodology described in Giglio et al. [1999]. Figure 3 shows the 90% detection probability curves estimated for VIIRS 750 m and MODIS 1 km fire data.
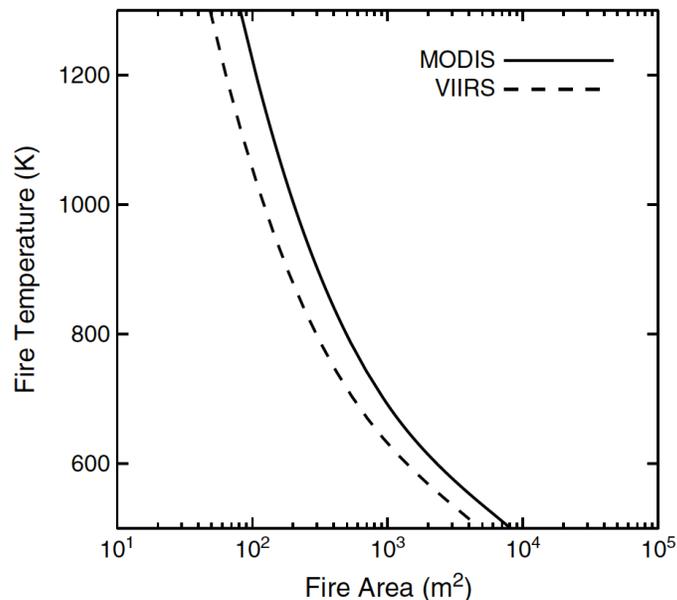

Figure 3: Theoretical 90% probability of fire detection curves derived for the VIIRS 750 m and MODIS 1 km fire algorithms as a function of fire area and temperature considering a boreal ecosystem background (adapted from Csiszar *et al.* [2014]).

4.2. VALIDATION APPROACH

The validation approach adopted for the VIIRS active fire data builds on the heritage EOS/MODIS methodology, which consisted on the use of coincident reference fire data derived from higher spatial resolution sensors [Morisette *et al.*, 2005; Schroeder *et al.*, 2008]. However, the early afternoon orbit described by VIIRS is a major impediment limiting the use of available Landsat-class sensors (typically on ≈10am orbits) due to prohibitively large temporal separation between same-day data acquisitions [Csiszar and Schroeder, 2008]. As an alternative, reference data

sets derived from airborne mapping instruments are used, complemented by field campaigns and other qualitative information originated from fire activity reports. Additionally, expert image analysts provide valuable input for the calculation of commission error rates associated with the occurrence of fire detection pixels in urban areas using available high-resolution visible imagery (e.g., Google Earth).

4.3. VALIDATION RESULTS

Data verification and validation was performed for selected sites across the globe, including dedicated field campaigns exploring small-to-medium size (<500 ha) prescribed fires (see for example: Dickinson *et al*. [2015]). Use of near-coincident airborne reference fire data shows good overall correspondence with VIIRS daytime and nighttime fire data generated for medium-to-large size wildfires as depicted in Figure 4.
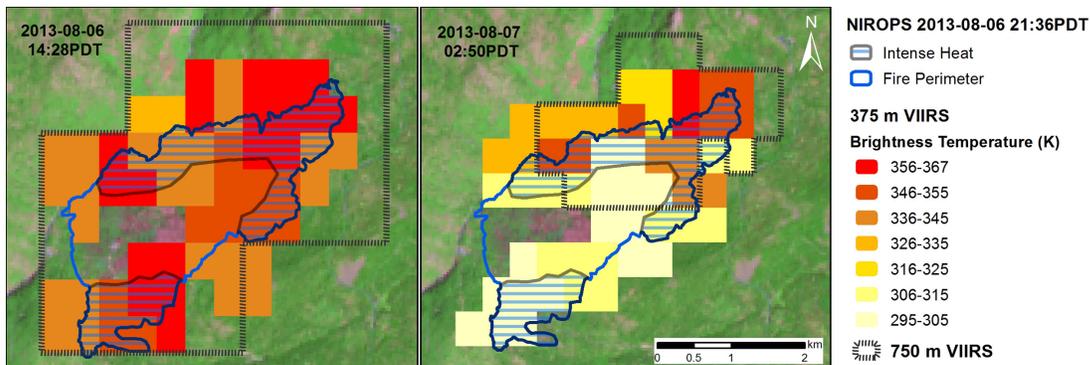

Figure 4: Airborne reference fire data (USDA/National Infrared Operations [NIROPs]) overlaid on near-coincident VIIRS daytime (left) and nighttime (right) fire detection data acquired on 06 and 07 August 2013, respectively. VIIRS 750 m fire pixel outline are displayed on top of 375 m fire pixels (filled polygons, color-coded according to brightness temperature)(adapted from Schroeder *et al*. [2014]).

Given the spectral resolution of the M13 channel, in particular concerning the partial overlap with a CO_2 absorption band in the 4 μm region, atmospheric attenuation effects may double compared, for example, to the corresponding MODIS mid-infrared data (channels 21/22) used in the MOD14/MYD14 products (Figure 5). While this characteristic could lead to systematic underestimation of VIIRS FRP values compared to coincident MODIS data, other factors such as pixel size/geometry, data aggregation and point spread function combine to create variable effects on FRP retrievals and the resulting correlation among products (Figure 6). Detailed assessment of FRP retrievals is currently limited to field validation campaigns that are few and sparse. Data verification and validation analyses shall expand as new reference data become available.
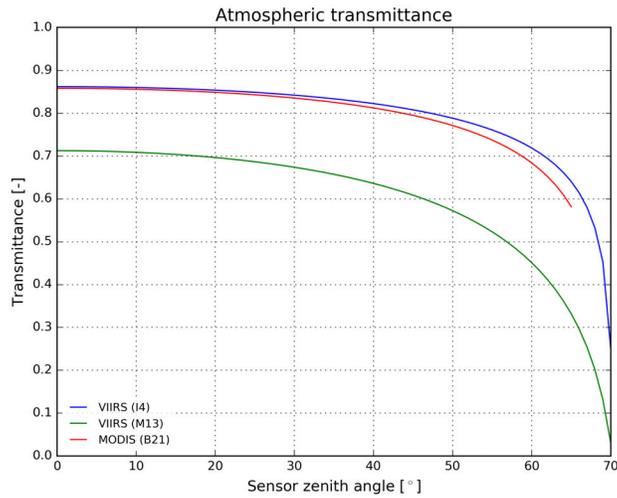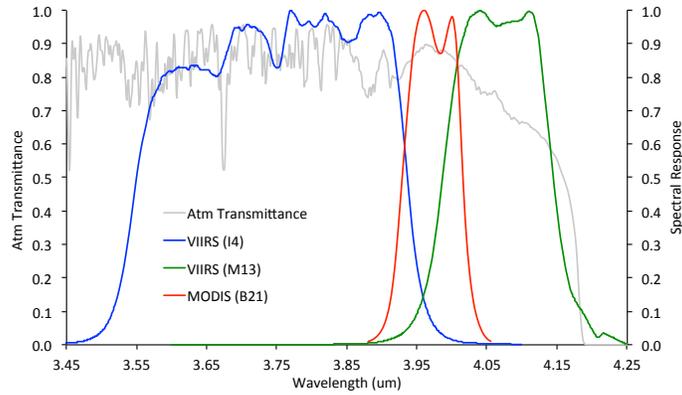
Figure 5: Spectral response functions for VIIRS I4 and M13, and MODIS B21/22 mid-infrared channels, and the corresponding atmospheric transmittance calculated using MODTRAN assuming U.S. standard atmospheric conditions (top panel). Bottom panel shows the corresponding net atmospheric transmittance as a function of the applicable VIIRS and MODIS sensor zenith angles.
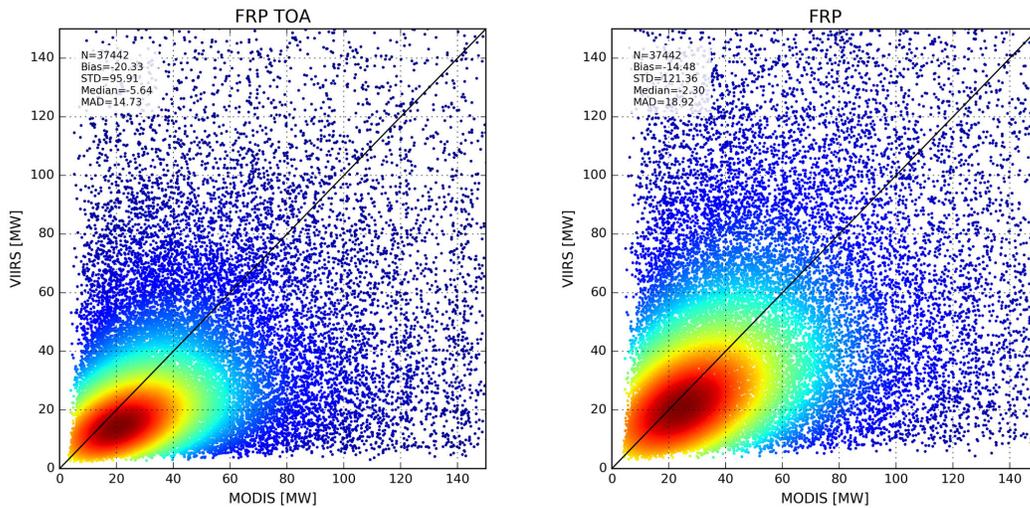

Figure 6: VIIRS M13 radiance-based FRP retrievals plotted against near-coincident Aqua/MODIS FRP (MYD14). Left panel shows top-of-atmosphere (TOA) data; right panel shows same data after atmospheric correction using MODTRAN® and MERRA 0.5º global analysis data.

5. USER GUIDANCE

VIIRS fire data users are encouraged to consult the data users guide for additional information on data accessibility and handling, and frequently asked questions.

6. ASSOCIATED PUBLICATIONS

Csiszar, I., Schroeder, W., Giglio, L., Ellicott, E., Vadrevu, K.,P., Justice, C.O., and Wind, B. (2014). Active fires from the Suomi NPP Visible Infrared Imaging Radiometer Suite: Product Status and first evaluation results. *Journal of Geophysical Research: Atmospheres*, doi: 10.1002/2013JD020453.

Giglio, L., Schroder, W., and Justice, C. (2016). The Collection 6 MODIS active fire detection algorithm and fire products. *Remote Sensing of Environment*, 178, 31-41.

Schroeder, W., Oliva, P., Giglio, L., and Csiszar, I. (2014). The new VIIRS 375 m active fire detection data product: Algorithm description and initial assessment. *Remote Sensing of Environment*, 143, 85-96.

7. REFERENCES

Csiszar, I., and Schroeder, W. (2008). Short-term observations of the temporal development of active fires from consecutive same-day ETM+ and ASTER imagery in the Amazon: Implications for active fire product validation. *IEEE Journal of Selected Topics in Applied Earth Observations and Remote Sensing*, 1(4), 248-253.

Cabrera, J., Cyamukungu, M., Stauning, P., Leonov, A., Leleux, P., Lemaire, J., *et al*. (2005). Fluxes of energetic protons and electrons measured on board the Oersted satellite. *Annales Geophysicae*, 23, 2,975-2,982.

Casadio, S., Arino, O., and Serpe, D. (2012). Gas flaring monitoring from space using ATSR instrument series. *Remote Sensing of Environment*, 116, 239-249.

Dickinson, M.B., Hudak, A.T., Zajkowski, T., Loudermilk, L.E., Schroeder W., *et al*. (2015). Measuring radiant emissions from entire prescribed fires with ground, airborne and satellite sensors – RxCADRE 2012. *International Journal of Wildland Fire*, doi: 10.1071/WF15090.

Giglio, L., Descloitres, J., Justice, C.O., and Kaufman, Y.J. (2003). An enhanced contextual fire detection algorithm for MODIS. *Remote Sensing of Environment*, 87, 273-282.

Giglio, L., Kendall, J.D., and Justice, C.O. (1999). Evaluation of global fire detection algorithms using simulated AVHRR infrared data. *International Journal of Remote Sensing*, 20 (10), 1947-1985.

Kaufman, Y.J., Justice, C.O., Flynn, L.P., Kendall, J.D., Prins, E.M., Giglio, L., et al. (1998). Potential global fire monitoring from EOS-MODIS. *Journal of Geophysical Research*, 103 (D24), 32,215-32,238.

Lobert, J.M., and Warnatz, J. (1993). Emissions from the combustion process in vegetation. In: *Fire in the Environment: The Ecological, Atmospheric, and Climatic*

Importance of Vegetation Fires (Editors: P.J. Crutzen and J.G. Goldammer), John Wiley & Sons Ltd.

Morisette, J.T., Giglio, L., Csiszar, I., and Justice, C.O. (2005). Validation of the MODIS active fire product over Southern Africa with ASTER data. *International Journal of Remote Sensing*, 26 (19), 4239-4264.

Schroeder, W., Prins, E., Giglio, L., Csiszar, I., Schmidt, C., Morisette, J.T,. and Morton, D. (2008). Validation of GOES and MODIS active fire detection products using ASTER and ETM+ data. *Remote Sensing of Environment*, 112, 2711-2726.

Wolfe, R.E., Lin, G., Nishihama, M., Tewari, K.P., Tilton, J.C., and Isaacman, A.R. (2013). Suomi NPP VIIRS prelaunch and on-orbit geometric calibration and characterization. *Journal of Geophysical Research: Atmospheres*, 118, doi:10.1002/jgrd.50873.

Wooster, M. J., Zhukov, B., and Oertel, D. (2003). Fire radiative energy for quantitative study of biomass burning: derivation from the BIRD experimental satellite and comparison to MODIS fire products. *Remote Sensing of Environment*, 86, 83–107.